Journal of Engineering and Technology for Industrial Applications

ITEGAM-JETIA

Manaus, v.8 n.37, p. 11-20. Sept./Oct., 2022

DOI: https://doi.org/10.5935/jetia.v8i37.830

ISSN ONLINE: 2447-0228

RESEARCH ARTICLE OPEN ACCESS

EFFECTS OF GRAPHITE ADDITION ON THE MECHANICAL PROPERTY AND WEAR RESISTANCE OF 60/40 BRASS

Chiedozie Valentine Oluigbo*[1], Johnson Olumuyiwa Agunsoye[2] and Joseph Babalola Agboola[3]

[1] Department of Welding and Fabrication Engineering Technology, Federal Polytechnic, Ilaro, Ogun State, Nigeria.
[2, 3] Department of Metallurgical and Materials Engineering, University of Lagos, Akoka, Lagos State, Nigeria.

[1] http://orcid.org/0000-0002-8900-2883, [2] http://orcid.org/0000-0002-8773-0051, [3] http://orcid.org/0000-0002-1359-7841

Email: *chiedozieoluigbo@gmail.com, jagunsoye@unilag.edu.ng, joeagboola@gmail.com

ARTICLE INFO

Article History
Received: October 09th, 2022
Accepted: October 27th, 2022
Published: October 31th, 2022

Keywords:
Brass,
Graphite,
Mechanical properties,
Nano-particulate,
Wear.

ABSTRACT

Brass 60/40 is widely used in a number of industrial applications where wear due to friction is a major concern. A significant number of failures in components such as bushings, gears, bearings and machine parts are due to wear. This study investigates the effects of Graphite nano-particulate on the mechanical properties and wear rate of 60/40 Brass produced by sand casting with varying graphite reinforcement addition ranging from 0.4 - 2.0 wt. %. The produced castings were characterized using XRD, SEM and TEM. The XRD revealed the formation of new phases such as Cu_5Zn_8 and $CuZn_2$ and the presence of free carbon within the microstructure. The wear rate of the composite specimens was evaluated using a pin-on-disc wear testing machine under dry conditions at room temperature. Taguchi's technique and analysis of variance method were used to study the influence of applied load, sliding speed, time and weight % composition on the wear rate. The results revealed that nano-particulate graphite-reinforced brass composite containing 2.0 wt. % graphite has the best wear resistance and applied load is the dominating factor on wear rate.

I. INTRODUCTION

In the manufacturing industry, wear is a severe problem. As a result, several efforts are being made to develop more durable materials and procedures to reduce tool and component wear. Wear has an estimated cost which vary from 1 to 4% of GDP [1]. It also accounts for approximately 75% of component or machine part failure [2]. Wear is the gradual loss of material from a machine's operating surface as a result of relative motion between the surfaces, while the resistance to relative motion between two adjacent bodies, either solids, liquids, or gas molecules, is known as friction [3]. Wear and friction are experienced by moving equipment parts. Lubrication can be applied by the introduction of a friction-reducing film [4] and as well as the use of improved materials to minimize friction and wear between moving surfaces in contact.

Brass is a copper-zinc alloy whose proportions can be varied to achieve different properties. Brass with 40 % of Zn is heterogeneous alloy with (α + β′) microstructure and it is also referred to as Muntz metal [5]. Most bearing materials are made of brass which eventually wears out over time and have to be replaced. Brass-based composites are now widely used in tribological engineering components, such as bearings and bushes. In this study, graphite powder in nanoscale is added to brass in order to improve its wear resistance property. Graphite is the most stable form of carbon under ordinary conditions. It also functions as a solid lubricant. Graphite's self-lubricating and dry lubricating properties are due to its crystal structure, and this makes it highly valued in industrial applications. Its usage as a brass alloy additive is also due to its low cost and environmental friendliness [6].

Composites are multiphase materials having desirable combinations of the best properties of the constituent phases. A Metal Matrix Composites (MMC) with nanoparticle reinforcement forms a Metal Matrix Nano-Composite (MMnC) [7]. Graphite brasses can be produced in different ways. Studies have shown that graphite brass can be prepared by graphitization annealing of cast brasses containing cementite particles, which were in-situ formed during the fasting process, and the graphite particles were formed by the decomposition of cementite particles in cast brasses [8]. In

addition, graphite brass can be produced by powder metallurgy and studies by Imai *et al.* [6] has shown that the addition of 1 weight percent graphite particle in the powder metallurgy extruded brass significantly improved the machinability. A copper-graphite composite's performance in terms of friction and wear was investigated by Ma *et al.* [9]. According to the authors, a rise in sliding speed causes a dramatic rise in the friction coefficient for a powder material containing 5 weight percent graphite. According to Kato *et al.* [10], adding graphite to anti-friction materials greatly improves their usability. In particular, composites containing 40% graphite had a remarkably low friction coefficient of 0.15. Rajkumar *et al.* [11] pointed out that the morphology of the friction surface depends on the material's composition and that a copper matrix composite material with a composition of 5 - 10% graphite has higher wear resistance. Further studies were also carried out on the electro-deposition of graphite-brass composite coatings. It was shown that the presence of graphite particles improved anti-friction properties of the composite coatings and that the composite coating containing approximately 3.7 volume % graphite had the best tribological properties [12]. In this current study, sand casting technique through the liquid metallurgy route was adopted to produce a nano-particulate graphite reinforced brass composite.

II. MATERIALS AND METHODS

II.1 MATERIALS

The materials used in this work include Brass, Copper, Zinc, and Graphite. Graphite lumps were sourced from Saman-Burkono in Ningi Local Government Area of Bauchi State, Nigeria. According to findings by Adeaoti *et al.* [13], Table 1 shows the results of the chemical analysis of the Saman-Burkono graphite head sample.

II.2 METHODS

II.2.1 Preparation of Graphite Nano-Particle

The Graphite lumps were crushed and ground to powder. It was later milled for 70 hours at 3,500 rev. per min. using laboratory ball mill of 1.11855 kilowatts, in order to reduce the ground graphite powder to nano-particulate size. The mechanical attrition was carried out at the Federal Institute of Industrial Research, Oshodi (FIIRO) in Lagos State, Nigeria. The graphite powder was analysed using the Transmission Electron Microscope (TEM).

II.2.2 Preparation of Brass Alloy

Commercial brass (60/40 brass) was gotten as scraps from Owode-Onirin, Lagos State, Nigeria. Pure Copper in bar and zinc scraps were also gotten from the same location, in order to supplement the masses of copper and zinc that will be lost by oxidation during melting of the brass. Table 2 shows the results of the compositional analysis of the brass.

In this research, the nano-particulate graphite reinforced brass composites were fabricated using the Liquid Metallurgy route via the sand-casting technique. Wooden patterns of cylindrical and rectangular shapes were constructed for this purpose. Melting of materials were done in a crucible furnace. The production of the composites was done with varying graphite reinforcement addition between 0.4 - 2.0 wt. %.

The characterization of the microstructure of the cast samples were carried out using X-Ray Diffraction (XRD) and Scanning Electron Microscope (SEM). Compositional analysis of the control sample was carried out using an S7 - Metal Lab Plus - Optical Emission Spectrometer. The samples' surfaces were ground and polished before the analysis.

II.3 MECHANICAL PROPERTY TESTING

II.3.1 Tensile Test

Tensile test was carried out according to ASTM D636, on the Universal Testing Machine, Model: SAUMYA D2. A load was applied continuously throughout on the test coupons with nominal dimension of 80 x 15 x 4 mm at a loading rate of 60 mm/min.

II.3.2 Hardness Test

Hardness test was carried out in accordance with ASTM A956 using a Brinell Hardness Testing machine. The test coupons were indented on the surface with a pin at different locations and the average of the results were taken from the display of the tester.

II.3.3 Impact Test

The impact energy test was carried out on Hounsfield Balanced Izod Impact Machine, Serial No: 3915 in accordance with ASTM D6110-10. The test coupons were prepared and inserted, then the hammer was thrown smartly and the readings were observed from the pointer, the impact energy were determined by taking the average of 2 coupons each per filler loading.

II.4 WEAR TEST

Wear test was done using Pin-On-Disc wear testing machine. It was conducted on the control sample as well as the 1.2% and 2.0% samples. The test was carried out in dry conditions and in accordance with ASTM G99 standard. Using an arm and weights attached to it, the pin specimen was pressed against the disk at a specific load. The parameters selected for the experiments were applied load, sliding speed, time and weight % reinforcement. The amount of wear was calculated by weighing the specimens both before and after the test. Volume loss in cubic millimeters was used to report wear results.

The experiments were conducted according to L9 Orthogonal array generated using Design of Experiments based on Taguchi's technique. The smaller-is-better (Signal to Noise ratio – S/N) performance characteristic was used to determine the wear rate (since the wear rate is expected to be minimized) as shown in equation 1. The experimental results were further analysed using Analysis of Variance to study the influence of each individual parameter on the response.

$$S/N = -10 * \mathrm{Log}[\sum(Y^2)/n] \quad (1)$$

Where Y = responses for the given factor level combination.
n = number of responses in the factor level combination.

III. RESULTS AND DISCUSSIONS

III.1 MICROSTRUCTURAL ANALYSIS

Table 2 shows the results of the spectrometric composition of the brass control sample. In order to examine the structure of the graphite, XRD and TEM were carried out as shown in figures 1 and 2 respectively. The XRD was able to identify the phases present as carbon, silicon and silicon dioxide. The TEM confirmed that the graphite powder is in nano-particulate size of 100 nanometers.

Table 1: Chemical characterization of Saman-Burkono Graphite head sample.

Compound	Al_2O_3	SiO_3	SO_3	K_2O	CaO	TiO_2	FeO_3	MgO
Composition (Wt. %)	4.35	67.14	BDL	3.70	2.89	0.40	0.38	0.15
Compound	V_2O_3	Cr_2O_5	MnO	PbO	Na_2O	ZnO	BaO	P_2O_5
Composition (Wt. %)	0.38	0.06	0.86	0.19	BDL	0.92	0.86	BDL

Source: Adeaoti *et al.* [13].
Abbreviation: BDL=below detection limit.

Table 2: Spectrometric compositional analysis of 60/40 Brass.

Element	Cu	Zn	Sn	Al	Si	Fe	Ni
Wt. % Composition	59	38.35	0.3	0.05	1.6	0.4	0.3

Source: Authors, (2022).

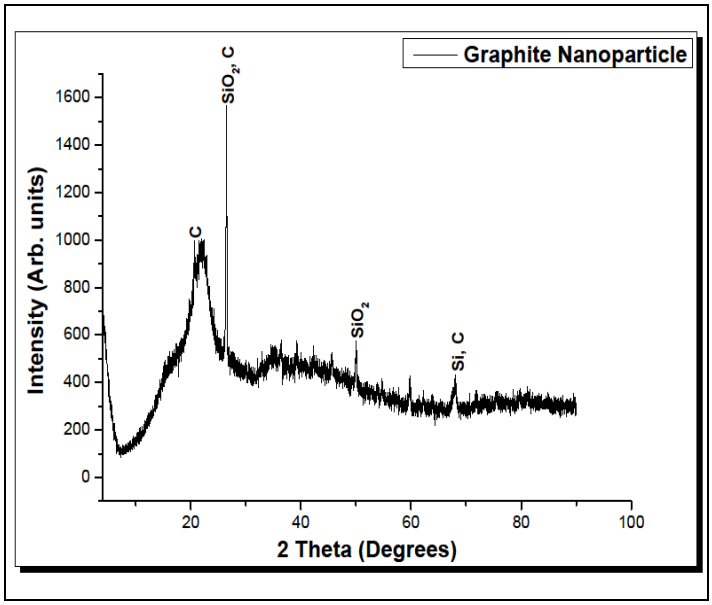

Figure 1: XRD of Graphite nanoparticles.
Source: Authors, (2022).

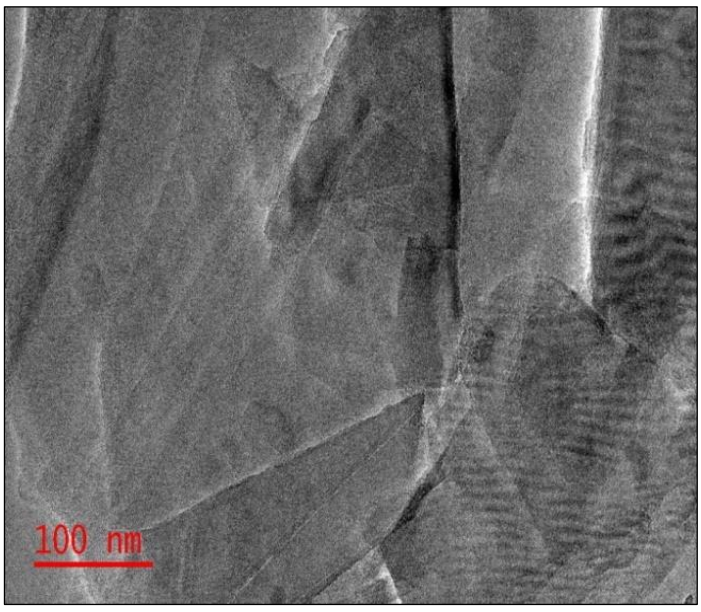

Figure 2: TEM of Graphite nanoparticles.
Source: Authors, (2022).

XRD and SEM examinations were carried out on the cast samples for the extreme compositions (control sample and 2 wt. % composite) and intermediate composition (0.4 wt. % composite). Figures 3 to 8 shows the XRD peak properties and SEM micrographs of the respective materials. The XRD of the control sample showed that the predominant phases were free Zn, CuZn, $CuZn_2$ while the SEM showed the morphologies of these phases. The XRD results in 0.4 wt. % composite and 2 wt. % composite identified free carbon in the form of graphite and Cu_5Zn_8 which is an intermetallic compound, in addition to other phases present.

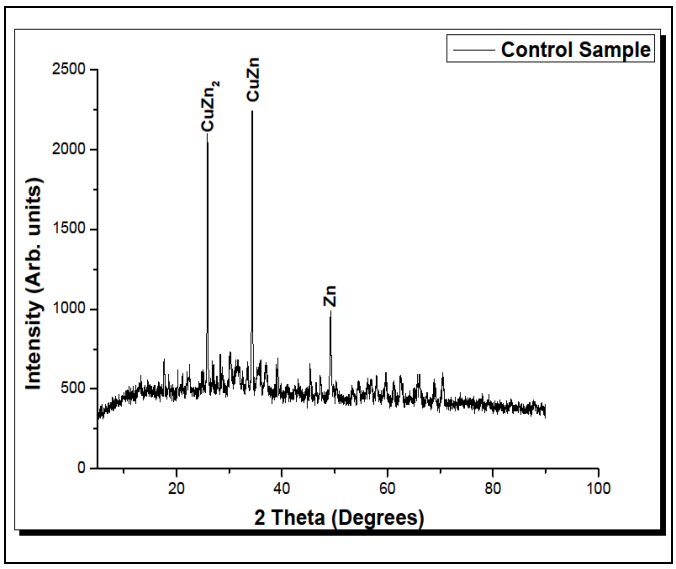

Figure 3: XRD of Control Sample.
Source: Authors, (2022).

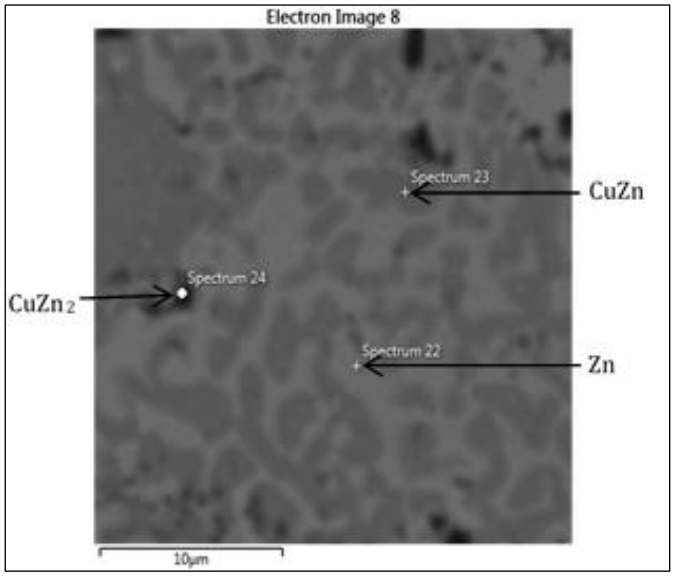

Figure 4: SEM Micrograph of Control Sample.
Source: Authors, (2022).

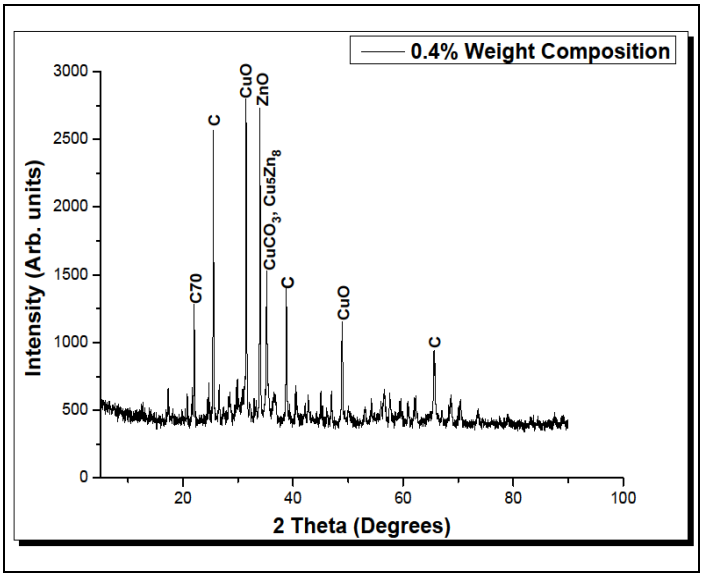

Figure 5: XRD of 0.4% sample.
Source: Authors, (2022).

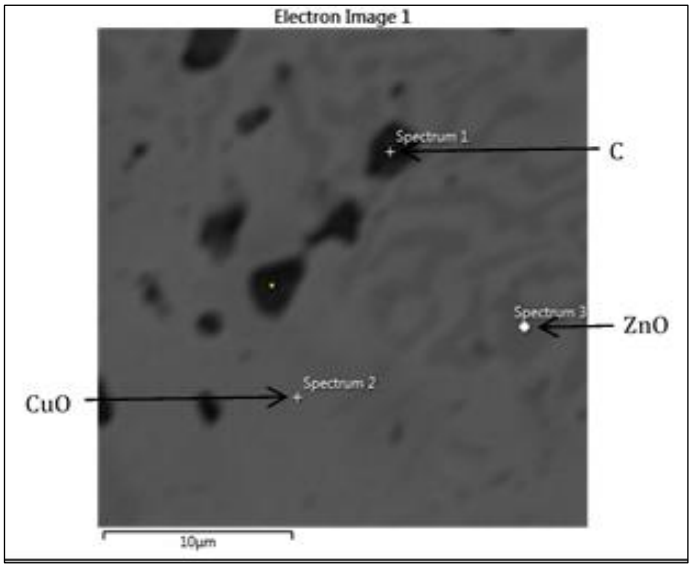

Figure 6: SEM Micrograph of 0.4% sample.
Source: Authors, (2022).

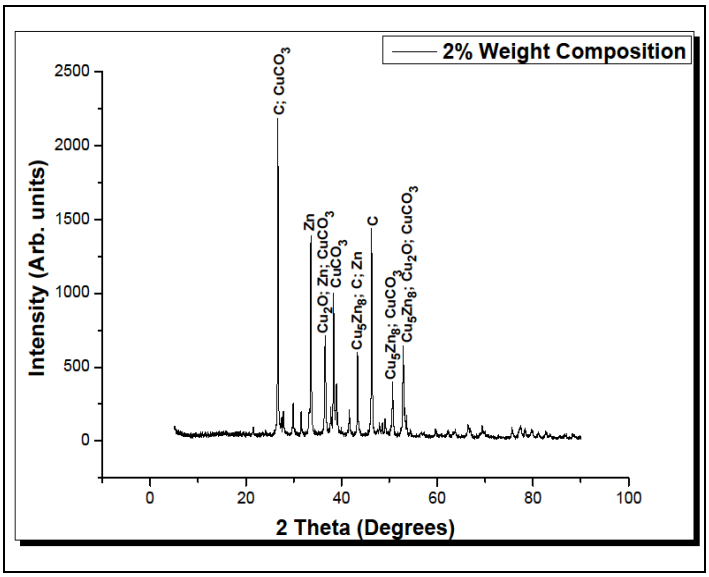

Figure 7: XRD of 2% sample.
Source: Authors, (2022).

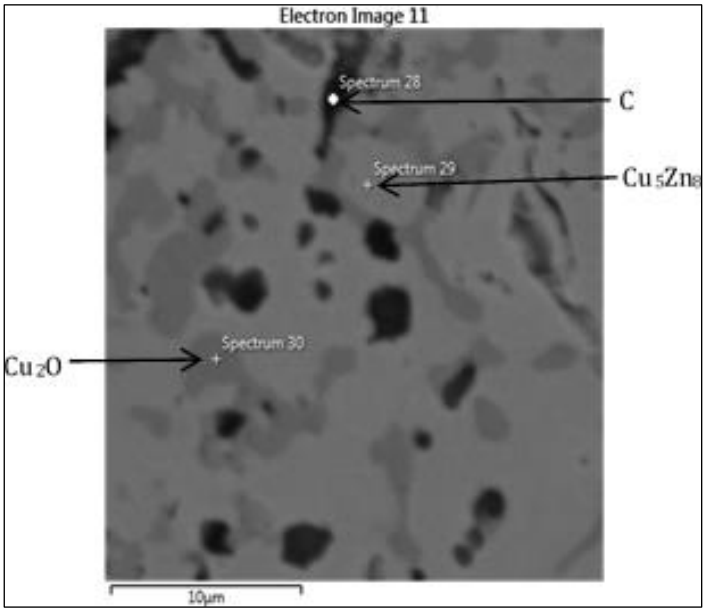

Figure 8: SEM Micrograph of 2% sample.
Source: Authors, (2022).

III.2 MECHANICAL PROPERTIES

The results of the mechanical properties of the brass reinforced composites are summarized in table 3.

Table 3: Mechanical Properties of Nano-Particulate Graphite Reinforced Brass Composite.

S (%)	UTS (MPa)	T (MPa)	E (MPa)	D (%)	I (J)	H (BHN)
Control	222.400	209.598	5728.500	13.555	18.460	19.900
0.4	238.930	157.836	6269.207	13.299	12.570	25.350
0.8	221.365	220.748	6550.185	12.076	11.820	25.900
1.2	232.474	142.296	6349.036	11.088	10.740	26.800
1.6	205.252	131.356	6119.281	9.802	10.480	26.600
2.0	268.775	243.990	7516.783	9.797	9.250	29.150

Abbrevation: S = Sample, UTS = Ultimate Tensile Strength, T = Tensile Strength at Break, E = Elastic Modulus, D = Ductility, I = Impact Energy, H = Hardness.

III.2.1 Toughness and Ductility

Figure 9 shows the relationship between the applied stress on the composite materials and the resulting strain (or elongation). It can be seen that the Control sample has the largest area under the stress-strain curve, hence has the highest toughness. The area under the stress-strain curve decreases as the weight percent addition of graphite nanoparticles in the brass matrix composite increase. It can also be seen from figure 10 that the Control sample has the highest ductility of 13.555% and it decreases as the weight percent addition of graphite nanoparticles in the brass matrix composite increase. This confirms the relationship between the toughness and ductility. It can be inferred that the addition of nano-particulate graphite reduced the toughness and ductility of brass matrix composite.

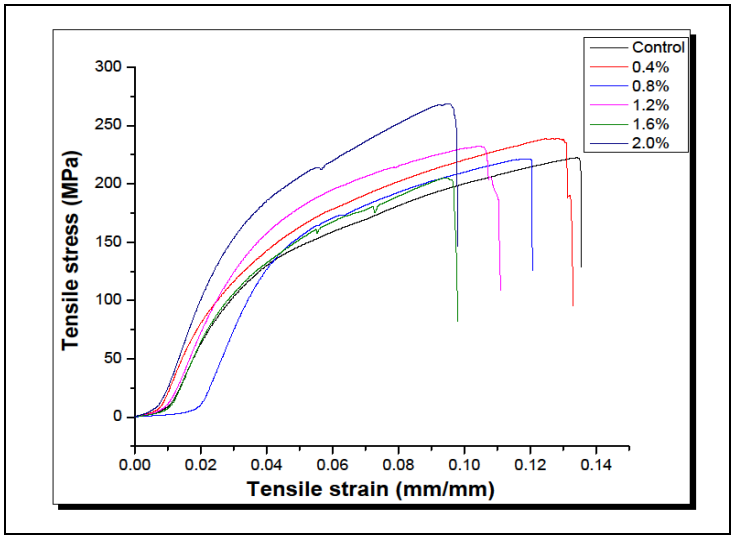

Figure 9: Tensile Stress against Tensile strain of the graphite nano-particulate reinforced brass composites.
Source: Authors, (2022).

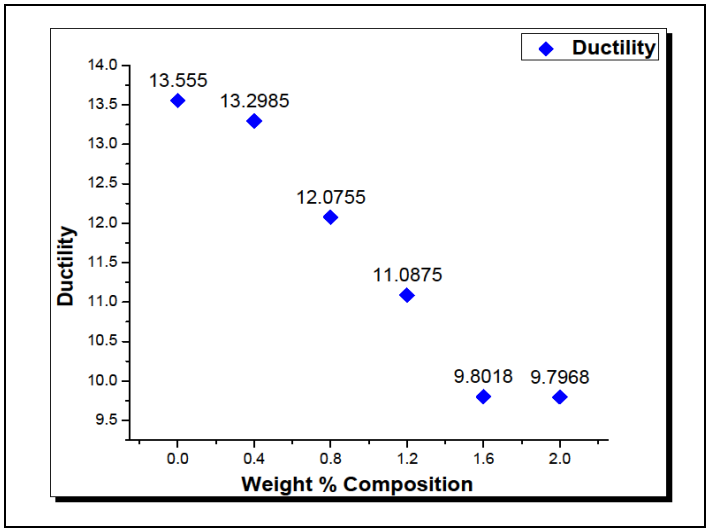

Figure 10: Ductility of the graphite nano-particulate reinforced brass composites.
Source: Authors, (2022).

III.2.2 Impact Energy

Figure 11 shows that the control sample has the highest impact energy and there was steady decrease in the impact energies as the weight percent addition of graphite nanoparticles in the brass matrix composite increased.

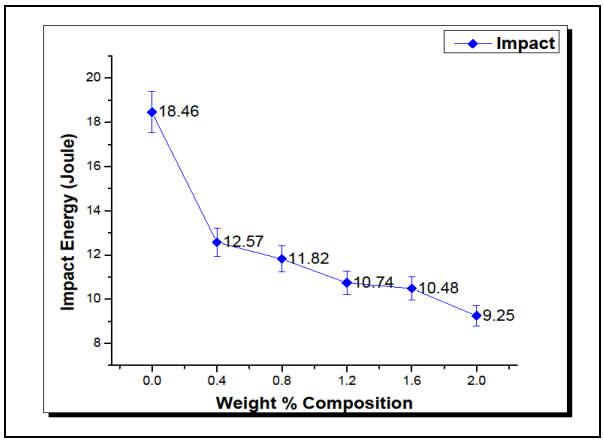

Figure 11: Impact Energy of the graphite nano-particulate reinforced brass composites.
Source: Authors, (2022).

III.2.3 Hardness

Figure 12 shows that the control sample has the lowest hardness value and this increases steadily as the weight percent addition of graphite nanoparticles in the brass matrix composite are increased.

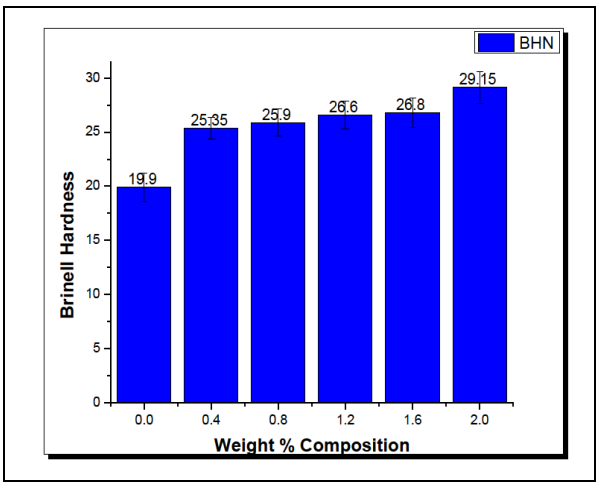

Figure 12: Brinell hardness of the graphite nano-particulate reinforced brass composites.
Source: Authors, (2022).

III.3 WEAR RATE ANALYSIS

III.3.1 Taguchi Analysis

Taguchi method was used to analyse the wear rate at low speed of 1.25m/s and high speed of 2.5m/s. Table 4 shows the wear process parameters and their values at different levels, while the wear rate values and S/Ns are displayed in Table 5. The S/N response table generated shows the influence of each parameter on the wear rate (Table 6 and Table 7). The strongest influencing parameter on the wear rate is determined using the delta value from these tables. The delta value gives the difference between the maximum and minimum value of each parameter level. The higher value of delta denotes that, the particular parameter has the strongest influence on the wear rate. From the delta value, it is noted that, load is the dominating factor on the wear rate followed by weight % composition and then time, for both the low speed and high speed.

Table 4: Process parameters and their values at different levels.

Process parameter	Low (1)	Medium (2)	High (3)
Load (N)	1.45	2.27	2.68
Time (Sec)	60	180	300
Material (Wt. %)	0	1.2	2.0

Source: Authors, (2022).

Table 5: Results of the wear rate and S/N ratios.

L (N)	T (S)	Wt. %	Low Speed (1.25m/s)		High Speed (2.5m/s)	
			W(g/m)	S/N	W(g/m)	S/N
1	1	1	0.039	48.18	0.0063	44.01
1	2	2	0.0024	52.40	0.016	35.92
1	3	3	0.0064	43.88	0.020	33.97
2	1	2	0.0026	51.70	0.0044	47.13
2	2	3	0.0083	41.62	0.0026	51.70
2	3	1	0.0019	54.43	0.0034	49.37
3	1	3	0.00085	61.41	0.0052	45.68
3	2	1	0.0015	56.48	0.0024	52.39
3	3	2	0.0027	51.37	0.0076	42.38

Source: Authors, (2022).

Abbreviation: L = Applied load, T = Time, W = Wear rate.

Table 6: Response Table for Signal to Noise Ratios at speed of 1.25m/s (Low speed).

Level	Load (N)	Time (Sec)	Wt. %
1	48.15	53.76	54.03
2	49.25	50.16	51.82
3	56.42	49.89	48.97
Delta	8.27	3.87	4.06
Rank	1	3	2

Source: Authors, (2022).

Table 7: Response Table for Signal to Noise Ratios at speed of 2.5m/s (High speed).

Level	Load (N)	Time (Sec)	Wt. %
1	37.97	45.61	48.59
2	49.40	46.67	41.81
3	46.82	41.91	43.79
Delta	11.43	4.76	6.78
Rank	1	3	2

Source: Authors, (2022).

Figures 13 and 14 show the main effect plot for SN ratio and mean respectively, at low speed. The slope of the line which connects between the levels clearly shows the power of influence of each control factor. In Figure 13, it is observed that optimal level for low wear rate is achieved by keeping the load at maximum level while the time and wt. % of reinforcement at minimum levels. The wear rate variation for each parameter when it changes from level to level is graphically represented in Figure 14.

In Figure 15 below, the lighter region shows low wear mass loss, that is, maximum wear resistance and the darker region shows high wear mass loss, that is, minimum wear resistance. Figure 16 shows the surface plot of wear rate against load and time at low speed.

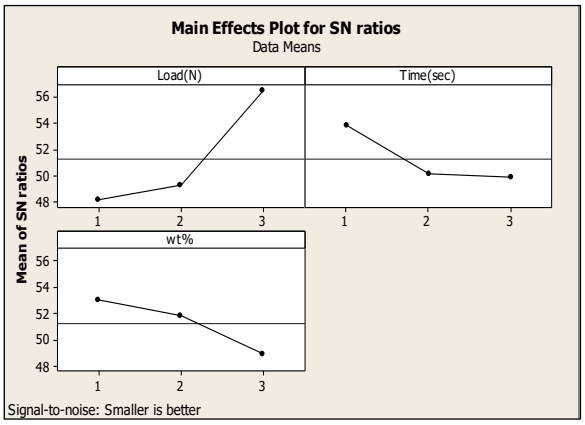

Figure 13: Main effect plots for SN ratio - Wear rate at low speed.
Source: Authors, (2022).

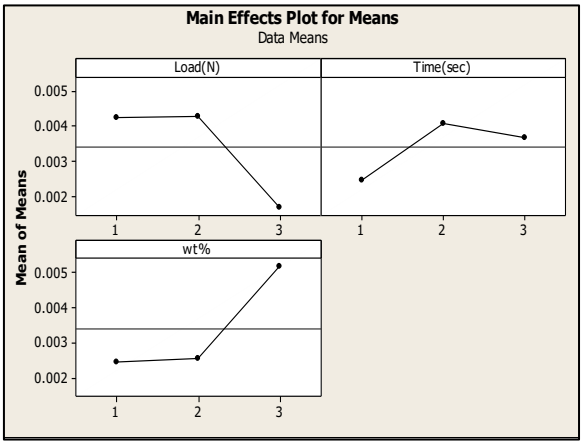

Figure 14: Main effect plots for means - Wear rate at low speed.
Source: Authors, (2022).

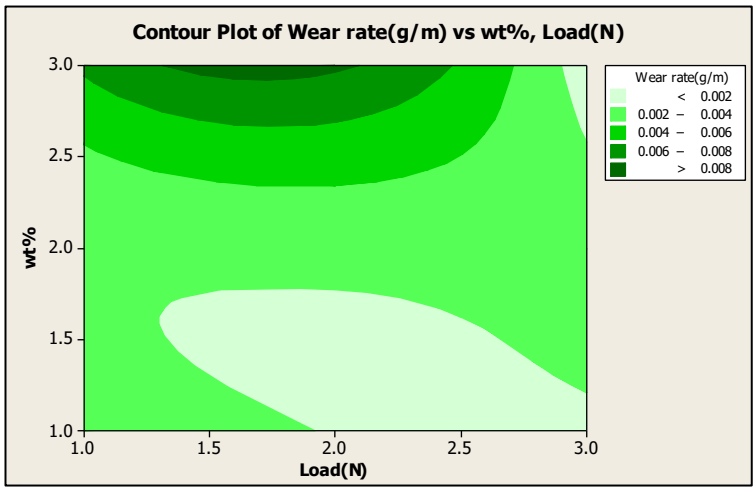

Figure 15: Contour plot of wear rate against weight % and load at low speed.
Source: Authors, (2022).

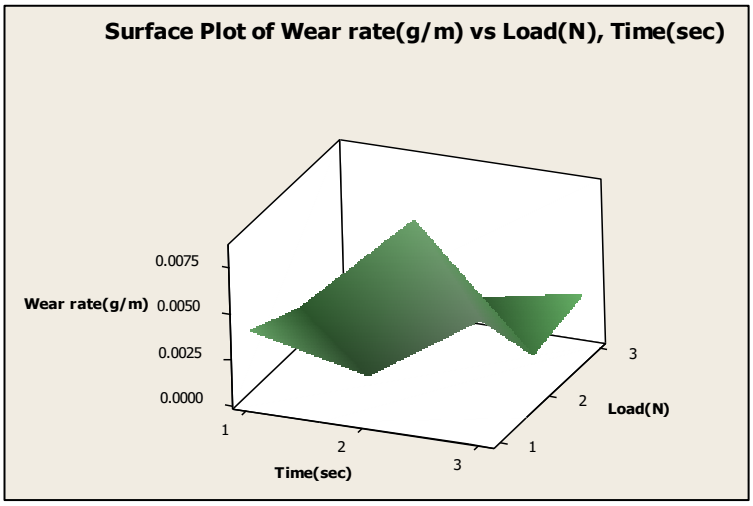

Figure 16: Surface plot of wear rate against load and time at low speed.
Source: Authors, (2022).

Figures 17 and 18 show the main effect plot for SN ratio and mean respectively, at high speed. In Figure 17, it is observed that optimal level for low wear rate is achieved by keeping the load and time at level 2 while the wt. % of reinforcement at minimum level. The wear rate variation for each parameter when it changes from level to level is graphically represented in Figure 18. The slope of the line which connects between the levels clearly shows the power of influence of each control factor.

Figure 19 shows the contour plot of wear rate against weight % and load at high speed while Figure 20 shows the surface plot of wear rate against load and time at high speed.

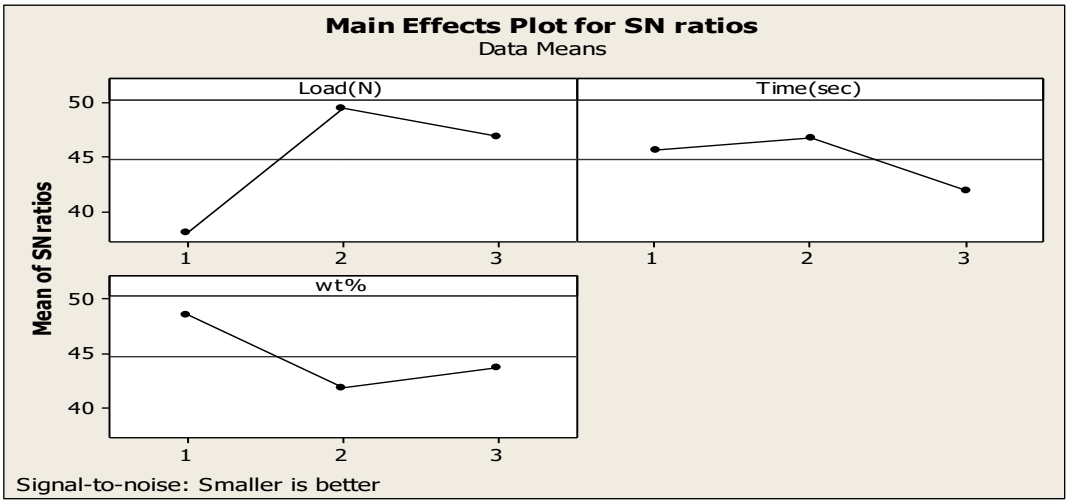

Figure 17: Main effect plots for SN ratio - Wear rate at high speed.
Source: Authors, (2022).

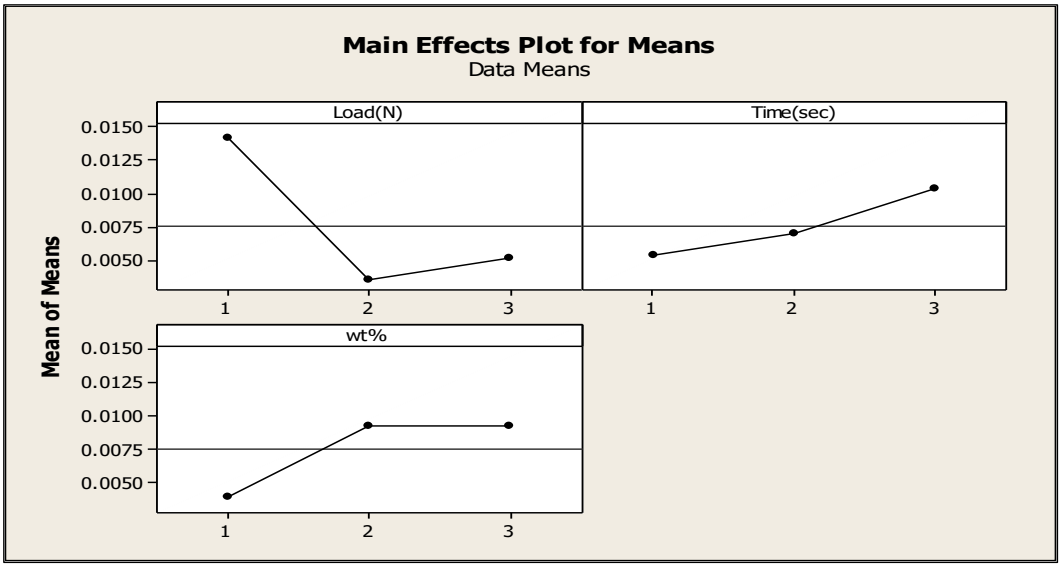

Figure 18: Main effect plots for means - Wear rate at high speed.
Source: Authors, (2022).

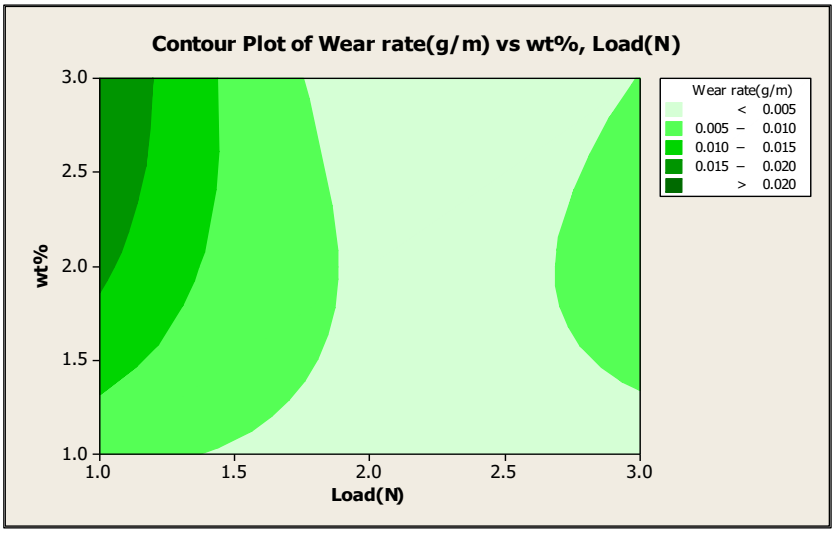

Figure 19: Contour plot of wear rate against weight % and load at high speed.
Source: Authors, (2022).

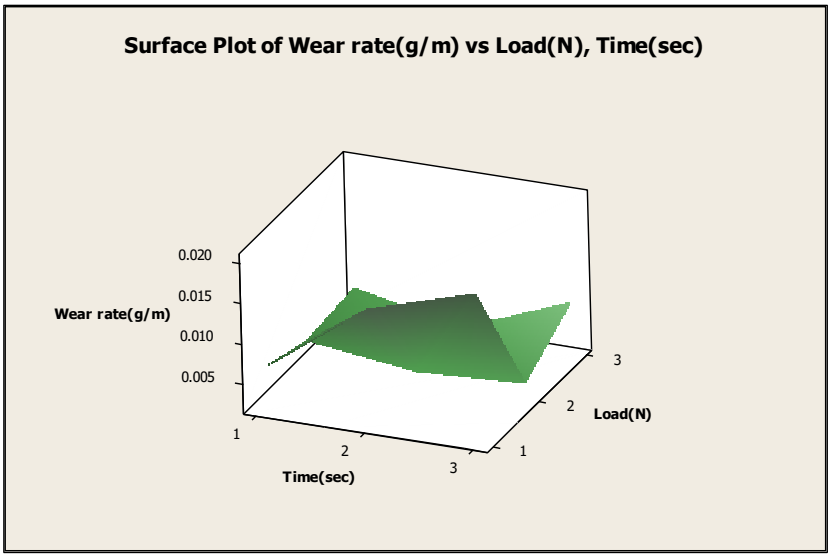

Figure 20: Surface plot of wear rate against load and time at high speed.
Source: Authors, (2022).

III.3.2 Analysis of Variance (ANOVA)

The percentage contribution of each parameter on the response was evaluated by using ANOVA. This analysis was carried out at a level of 5% significance with a confidence level of 95%. The results of the ANOVA on the wear rate at low speed are displayed in Table 8. It was observed that the applied load has a higher contribution of 69.01%, followed by the time with 16.20% and wt. % with 14.79%. Likewise, the results of the ANOVA on the wear rate at high speed are displayed in Table 9. It was observed that the applied load has a higher contribution of 66.12%, followed by the wt. % with 22.40% and time with 11.50%.

Table 8: Analysis variance results for low speed.

Source	DF	SS	MSS	F	P	% Contribution
Applied load	2	121.06	60.53	0.98	0.505	69.01
Time (s)	2	28.03	14.01	0.23	0.815	16.20
Wt. %	2	26.07	13.03	0.21	0.826	14.79
Error	2	123.62	61.81			
Total	8	298.77				

Source: Authors, (2022).

Table 9: Analysis variance results for high speed.

Source	DF	SS	MSS	F	P	% Contribution
Applied load	2	215.637	107.818	24.77	0.039	66.12
Time (s)	2	37.456	18.728	4.30	0.189	11.50
Wt. %	2	73.007	36.504	8.39	0.107	22.40
Error	2	8.706				
Total	*8*	*334.805*				

Source: Authors, (2022).

IV. CONCLUSIONS

The effects of Nano-particulate Graphite addition on the Tribological property of 6040 brasses for industrial applications was investigated. Based on the outcome of the research, the following conclusions are drawn from this study:

i. The nano-particulate graphite reinforced brass composites have been successfully produced by the stir casting route.
ii. The ductility, impact energy and toughness values of the brass matrix composite decreased with the increase in weight percent of graphite nano-particulate powder while the hardness values increased slightly with an increase in weight percent of graphite nano-particulate powder.
iii. At low speed of 1.25 m/s, the optimum process parameters which results in minimum wear rate are applied load of 2.68N, time of 60 sec and 2 wt. % of reinforcement. At low speed, load has the highest percentage contribution (69.01%) on the wear rate followed by time (16.20%) and wt. % of reinforcement (14.79%).
iv. At high speed of 2.5m/s, the optimum process parameters which results in minimum wear rate are applied load of 2.27N, time of 180sec and 2 wt. % of reinforcement. Hence, 2 wt. % of graphite reinforcement has the best wear resistance in the brass matrix composites. At high speed, load has the highest percentage contribution (66.12%) on the wear rate followed by wt. % of reinforcement (22.40%) and time (11.50%).

V. AUTHOR'S CONTRIBUTION

Conceptualization: Johnson Olumuyiwa Agunsoye.
Methodology: Chiedozie Valentine Oluigbo and Johnson Olumuyiwa Agunsoye.
Investigation: Chiedozie Valentine Oluigbo and Johnson Olumuyiwa Agunsoye.
Discussion of results: Chiedozie Valentine Oluigbo, Johnson Olumuyiwa Agunsoye and Joseph Babalola Agboola.
Writing – Original Draft: Chiedozie Valentine Oluigbo.
Writing – Review and Editing: Chiedozie Valentine Oluigbo, Johnson Olumuyiwa Agunsoye and Joseph Babalola Agboola.
Resources: Chiedozie Valentine Oluigbo and Johnson Olumuyiwa Agunsoye.
Supervision: Johnson Olumuyiwa Agunsoye and Joseph Babalola Agboola.
Approval of the final text: Chiedozie Valentine Oluigbo, Johnson Olumuyiwa Agunsoye and Joseph Babalola Agboola.

VI. REFERENCES

[1] S. Thota, S. K. Dalaa, S. C. Goud, "A Dissertation on Wear Behaviour of Aluminium & Brass," *International Journal of Research in Engineering and Applied Sciences*, vol. 5, no. 11, Nov. 2015.

[2] M. S. Khan, Z. Hasan, S. M. Farhan, "Effect of Orientation and Applied Load on Abrasive Wear Property of Brass 60:40," *Journal of Minerals and Materials Characterization and Engineering*, vol. 2, no. 1, pp. 49-53, Jan. 2014, doi: 10.4236/jmmce.2014.21008.

[3] S. J. Patil, D. P. Patil, A. P. Shrotri, V P. Patil, "A Review on Effect of addition of Nano Particles on Tribological properties of Lubricants," *International Journal*

of Mechanical Engineering and Technology (IJMET), vol. 5, no. 11, pp. 120-129, Nov. 2004.

[4] R. Gaur, A. Kumar, A. Suhane, "Effect of Addition of Nano Particles on Tribological Properties of Lubricants - A Review," *International Research Journal of Engineering and Technology (IRJET)*, vol. 5, no. 5, May 2018.

[5] R. Konečná, S. Fintová, *Copper and Copper Alloys: Casting, Classification and Characteristic Microstructures, in Copper Alloys - Early Applications and Current Performance – Enhancing Processes*, Dr. Luca Collini, Ed., Publishers InTech, Žilina, Slovak Republic, 2012.

[6] H. Imai, K. Kondoh, G. Katano, Y. Kosaka, A. Kojima, "Characteristics of lead-free powder metallurgy Cu60-Zn40 Brass Alloys with Graphite," *Transaction of TWRI*, vol. 37, no.1, Jul. 2008.

[7] R. Casati, M. Vedani, "Metal Matrix Composites Reinforced by Nano-Particles - A Review," *Metals*, vol. 4, no. 1, pp. 65-83, Mar. 2014, doi: 10.3390/met4010065.

[8] H. Zhuo, J. Tang, Y. Xue, N. Ye, "Preparation of lead-free free-cutting graphite brasses by graphitization of cementite," *Transactions of Nonferrous Metals Society of China*, vol. 25, no. 10, pp. 3252 – 3257, Mar. 2015, doi: 10.1016/S1003-6326(15)63961-9.

[9] W. L. Ma and J. J. Lu, "Effect of sliding speed on surface modification and tribological behavior of copper–graphite composite," *Tribology Letters*, vol. 41, pp. 363-370, Nov. 2011, doi: 10.1007/s11249-010-9718-x.

[10] H. Kato, M. Takama, Y Iwai, K. Washida and Y. Sasaki, "Wear and mechanical properties of sintered copper–tin composites containing graphite or molybdenum disulfide," *Wear*, vol. 255, pp. 573-578, 2003, doi:10.1016/S0043-1648(03)00072-3.

[11] K. Rajkumar and S. Aravindan, "Tribological performance of microwave sintered copper–TiC–graphite hybrid composites," *Tribology International*, vol. 44. pp. 347–358, 2011, doi: 10.1016/j.triboint.2010.11.008.

[12] M. Ghorbani, M. Mazaheri, K. Khangholi, Y. Kharazi, "Electrodeposition of graphite-brass composite coatings and characterization of the tribological properties," *Surface and Coatings Technology*, vol. 148, no. 1, pp. 71-76, Jun. 2001, doi:10.1016/S0257-8972(01)01322-6.

[13] M. O. Adeoti. O. A. Dahunsi, O. O. Awopetu, F.O. Aramide, O. O. Alabi, and A. S. Abdulkareem, "Characterization of Saman-Burkono (Nigeria) Graphite for Crucible Production," *Journal of Engineering and Engineering Technology*, vol. 13, pp. 20-29, Feb. 2019.